J Neurophysiol 90: 2964–2972, 2003.
First published July 16, 2003; 10.1152/jn.00172.2003.

Membrane Potential of CA3 Hippocampal Pyramidal Cells During Postnatal Development

Roman Tyzio,[1,*] Anton Ivanov,[1,*] Cristophe Bernard,[1] Gregory L. Holmes,[2] Yehezkiel Ben-Ari,[1] and Roustem Khazipov[1,2]

[1]*Institut de la Neurobiologie de la Méditterranée-Institute National de la Santé et de la Recherche Médicale U29, Marseille, France and* [2]*Division of Neurology, Neuroscience Center at Dartmouth, Dartmouth Medical School, Lebanon, New Hampshire 03756*

Submitted 25 February 2003; accepted in final form 12 June 2003

Roman, Tyzio, Anton Ivanov, Christophe Bernard, Gregory L. Holmes, Yehezkiel Ben-Ari, and Roustem Khazipov. Membrane potential of CA3 hippocampal pyramidal cells during postnatal development. *J Neurophysiol* 90: 2964–2972, 2003. First published July 16, 2003; 10.1152/jn.00172.2003. A depolarized resting membrane potential has long been considered to be a universal feature of immature neurons. Despite the physiological importance, the underlying mechanisms of this developmental phenomenon are poorly understood. Using perforated-patch, whole cell, and cell-attached recordings, we measured the membrane potential in CA3 pyramidal cells in hippocampal slices from postnatal rats. With gramicidin perforated-patch recordings, membrane potential was −44 ± 4 (SE) mV at postnatal days P0–P2, and it progressively shifted to −67 ± 2 mV at P13–15. A similar developmental change of the membrane potential has been also observed with conventional whole cell recordings. However, the value of the membrane potential deduced from the reversal potential of *N*-methyl-D-aspartate channels in cell-attached recordings did not change with age and was −77 ± 2 mV at P2 and −77 ± 2 mV at P13–14. The membrane potential measured using whole cell recordings correlated with seal and input resistance, being most depolarized in neurons with high, several gigaohms, input resistance and low seal resistance. Simulations revealed that depolarized values of the membrane potential in whole cell and perforated-patch recordings could be explained by a shunt through the seal contact between the pipette and membrane. Thus the membrane potential of CA3 pyramidal cells appears to be strongly negative at birth and does not change during postnatal development.

INTRODUCTION

During brain development, morphological differentiation of neurons is accompanied by major changes in their functional properties (Ben-Ari et al. 1997; Spitzer 1979). One universally accepted observation is that early in development, immature neurons from virtually all brain structures studied using intracellular or whole cell recordings display a strongly depolarized—compared with adult neurons—resting membrane potential (E_m). While in mature cortical neurons the E_m ranges from −65 to −85 mV (Spruston and Johnston 1992; Staley et al. 1992), in the immature neurons the E_m is typically more positive by tens of millivolts. Thus the E_m in the neonatal rat hippocampal pyramidal neurons ranges from –30 to −67 mV (Ben-Ari et al. 1989; Lamsa et al. 2000; Psarropoulou and Descombes 1999; Spiegelman et al. 1992; Zhang et al. 1991). In the embryonic and early postnatal rat neocortex, the E_m of cortical plate neurons is within the range from –35 to −65 mV (LoTurco et al. 1991); for newborn layers I–III neocortical neurons, the E_m is around −40 to –50 mV (Burgard and Hablitz 1993; Mienville and Pesold 1999; Zhou and Hablitz 1996). Measurements in somatosensory cortex revealed an E_m of −40 to –50 mV in Cajal-Retzius cells, bifurcated pyramidal neurons, multipolar and bipolar neurons, and immature pyramidal cells (Luhmann et al. 2000). A similar range of the resting membrane potentials has also been reported for the chick hair cells at E10–12 (around –50 mV) (Masetto et al. 2000) and perinatal rat phrenic motoneurons (from −49 to –59 mV) (Martin-Caraballo and Greer 1999). In guinea pig celiac neurons at birth, the E_m is around −55 mV, whereas early fetal celiac neurons have an E_m of only –20 to –30 mV (Anderson et al. 2001). At birth, rat nucleus accumbens neurons have an E_m around –50 mV (Belleau and Warren 2000). Thus the depolarized value of the neuronal membrane potential appears to be a general feature of immaturity.

Despite of the ubiquity of the depolarized membrane potential recorded in immature neurons using intracellular or whole cell recordings and the major impact it may have on neuronal excitability, underlying mechanisms remain poorly understood. Because the value of the resting membrane potential is determined by ionic gradients and membrane permeability, it has been proposed that delayed development of the ionic transporters and channels may contribute to the depolarized values of the membrane potential in immature neurons. In particular, a developmental increase in the potassium conductance and decrease in the chloride permeability together with a decrease in the intracellular chloride concentration have been emphasized (Ben-Ari et al. 1989; Spiegelman et al. 1992; Wang et al. 2001; Zhang et al. 1991).

Intracellular recordings with sharp electrodes and whole cell and perforated-patch recordings with patch electrodes are commonly used to assess the value of the membrane potential. However, both techniques introduce several sources of error. These include liquid junction potentials, modification of intracellular composition that can affect the ionic gradients and the activity of ionic channels, and a short-circuit effect of the leak

*R.Tyzio and A. Ivanov contributed equally to this work.

Address for reprint requests and other correspondence: R. Khazipov, Div. of Neurology, Dartmouth Medical School, One Medical Center Dr., Lebanon, NH 03756 (E-mail: roustem.khazipov@dartmouth.edu).

The costs of publication of this article were defrayed in part by the payment of page charges. The article must therefore be hereby marked "*advertisement*" in accordance with 18 U.S.C. Section 1734 solely to indicate this fact.

through the contact between the electrode and the membrane (Barry and Lynch 1991; Marty and Neher 1995; Spruston and Johnston 1992; Staley et al. 1992; Velumian et al. 1997). Leak resistance is ~500 MΩ in recordings with sharp electrodes and it is increased to several gigaohms in patch-clamp recordings. However, in a small cell with several gigaohms of resistance, a leak through the seal between the patch pipette and membrane may introduce an important error in the measurement of E_m using whole cell recordings (Barry and Lynch 1991). Therefore it is conceivable that depolarized values of the resting membrane potential in immature neurons are simply due to the short-circuit effect of the leak through the contact between the electrode and the membrane in the invasive recordings.

In the present study, we estimated the membrane potential of CA3 pyramidal cells during their postnatal development using whole cell, gramicidin perforated-patch, and cell-attached recordings of *N*-methyl-D-aspartate (NMDA) channels. We report that whole cell and gramicidin perforated-patch recordings give similar estimates of the membrane potential, which is strongly depolarized at birth (−44 mV) and hyperpolarizes to −67 mV at the end of the second postnatal week. However, the membrane potential deduced from cell-attached recordings of NMDA channels is more negative, around –77 mV, and does not change during postnatal development. Simulations revealed that depolarized values of the membrane potential in whole cell recordings could be explained, at least in part, by the shunting through the contact between the patch pipette and the membrane, which affects measurements, particularly in small neurons that have high resistances in the gigaohm range. Thus the membrane potential of CA3 pyramidal cells appears to be strongly negative at birth and does not change during postnatal development.

METHODS

Experimental system

Hippocampal slices were prepared from postnatal days (P) P0–26 Wistar rats of both sexes. All animal protocols conformed to the French Public Health Service policy and the INSERM guidelines on the use of laboratory animals. Animals were anesthetized with chloral hydrate (350 mg/kg, ip) and decapitated. Brains were removed and transverse hippocampal slices (350–500 μm) were cut using the Vibratome (VT 1000E; Leica, Nussloch, Germany). Slices were kept in oxygenated (95% O_2-5% CO_2) artificial cerebrospinal fluid (ACSF) of the following composition (in mM): 126 NaCl, 3.5 KCl, 2.0 $CaCl_2$, 1.3 $MgCl_2$, 25 $NaHCO_3$, 1.2 NaH_2PO_4, and 11 glucose (pH 7.4) at room temperature (20–22°C) ≥1 h before use. For recordings, slices were placed into a conventional fully submerged chamber superfused with ACSF (30–32°C) at a rate of 2–3 ml/min.

Electrophysiological recordings and data analysis

Patch-clamp recordings were performed using Axopatch 200A (Axon Instruments, Union City, CA) and EPC-9 (HEKA Elektronik, Lambrecht/Pfalz, Germany) amplifiers. Patch electrodes were made from borosilicate glass capillaries of 1.5 mm OD and 0.86 ID (GC150F-15, Clark Electromedical Instruments, Pangbourne, UK). The tip of the patch pipettes was of 1–2 μm. Patch pipette solution for whole cell recordings contained (in mM) 135 potassium gluconate, 13 NaCl, 1 $MgCl_2$, 0.1 $CaCl_2$, 1 EGTA, and 10 HEPES; pH 7.2. When filled with this solution, the pipettes had a resistance from 5 to 12 MΩ. Seal resistance was on average 10.7 ± 3.7 GΩ (n = 20). Membrane potential was measured 5–15 min after breaking to whole cell. The average membrane potential (E_m) was determined as a mean value of the membrane potential obtained during a recording of ≥2 min in current-clamp mode with null current. Membrane potentials were corrected for liquid junction potential of 7 mV. Patch pipette solution for gramicidin perforated-patch recording contained (in mM) 150 KCl and 10 HEPES, buffered to pH 7.2 with Tris-OH. Gramicidin was first dissolved in DMSO to prepare a stock solution of 10–40 mg/ml and then diluted to a final concentration of 80 μg/ml in the pipette solution. The gramicidin-containing solution was prepared and sonicated <1 h before the experiment. Patch pipettes were backfilled with a gramicidin-containing solution, and then the tip of the pipettes was dipped into and filled with a gramicidin-free solution by applying a negative pressure for 20–30 s to facilitate cell-attached formation (seal resistance: 4.1 ± 2.0 GΩ). Twenty to 30 min after the cell-attach formation, series resistance decreased and stabilized at 48.2 ± 2.8 MΩ (range: 8–60 MΩ). Values of the membrane potential were corrected for series resistance during analysis. Input resistance (R_{in}) and capacitance were determined from the analysis of responses to hyperpolarizing steps of −5/−20 mV applied from the holding potential of −80 mV; in this range, the *I-V* curve of cells was close to linear.

For cell-attached recordings of NMDA channels, the tip of patch pipettes was covered with a wax to reduce capacitance. Pipettes were filled with nominally magnesium-free ACSF containing 10 μM NMDA and 10 μM glycine. Analysis of activity of NMDA channels was performed using the Axon software package as described earlier (Khazipov et al. 1995). Both multilevel and short (<2 ms) openings were discarded during analysis.

Extracellular field potentials were recorded using electrodes made from 50-μm-diam tungsten wire. Electrodes were positioned in the pyramidal cell layer of the CA3 subfield, and signals were amplified using a custom made amplifier (band-pass: 0.1 Hz to 4 kHz; ×1,000). For single action potential detection, records were filtered with a RC (single pole) high-pass filter at >200 Hz.

Recordings were digitized (10 kHz) on-line using a Digidata 1200 interface card (Axon Instruments, Union City, CA) and analyzed off-line with the Axon software package, Mini Analysis program (Synaptsoft), and Origin 5.0 (Microcal Software, Northampton, MA). Group measures are expressed as means ± SE; error bars also indicate SE. The statistical significance of differences was assessed with the Student's *t*-test. The level of significance was set at $P < 0.05$.

RESULTS

Gramicidin perforated-patch and whole cell recordings

Gramicidin perforated-patch recordings (Ebihara et al. 1995; Horn and Marty 1988) were obtained from 108 CA3 pyramidal cells at postnatal ages of P0–26. Typical traces of current-clamp recordings at P0, P2, P8, and P14 are shown in Fig. 1. In the majority of recorded neurons, membrane potentials were not stable and displayed various fluctuations that often gave rise to action potentials. Therefore the resting membrane potential was measured as an *average* membrane potential from recordings in current-clamp mode with null current injected. Examples of the all-points histograms of the membrane potential are shown on Fig. 1. Although the values of the membrane potential varied significantly over time in each given neuron as well as between neurons at a given age (Fig. 2), average values of membrane potential were significantly more depolarized in neurons from the younger rats. Thus neurons from the most immature group (P0–2) had an average membrane potential

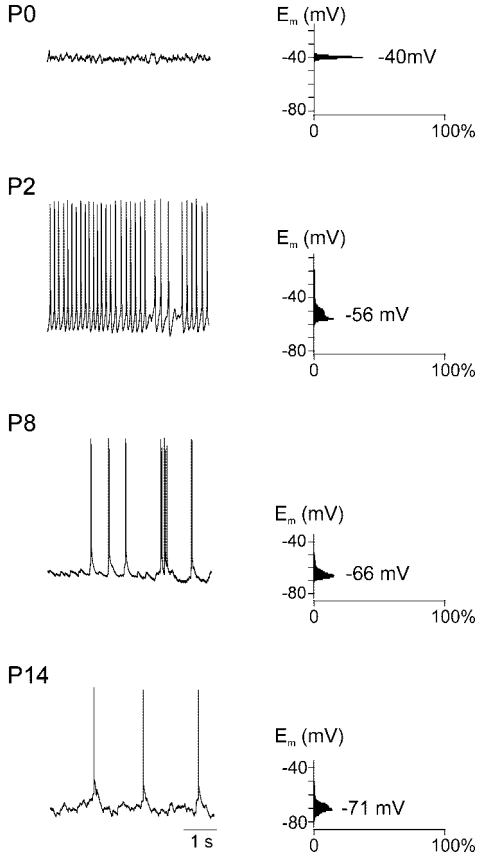

FIG. 1. Gramicidin perforated-patch recordings from CA3 pyramidal cells at various postnatal ages. Traces represent recordings in current-clamp mode with null current injected. *Right*: corresponding all point histograms of the membrane potentials obtained from 2-min recordings (acquisition: 10 kHz, bin = 0.5 mV). Values of average resting membrane potentials are indicated near the histograms. Vertical scales of the histograms also serve as voltage scales for the traces. Ages of rats are indicated on the left in postnatal days (P).

-44 ± 4 mV ($n = 18$). The most immature neurons typically fired no action potentials either spontaneously (Fig. 1) or in response to depolarization unless prehyperpolarized to a more negative potential (not shown), suggesting that they were in a state of depolarization block. During the first two postnatal weeks, average membrane potential progressively shifted toward negative values to attain a value of -67 ± 2 mV at P13–15 ($n = 18$). Developmental changes in the membrane potential were paralleled by a progressive decrease of input resistance and increase of capacitance (Fig. 2). At P0–2, input resistance was 2.6 ± 0.4 GΩ and capacitance was 33 ± 5 pF ($n = 18$); at P13–15: 0.25 ± 0.04 GΩ and 166 ± 5 pF, respectively ($n = 18$). It is likely that developmental decreases of input resistance and increases of capacitance reflect growth of CA3 pyramidal cells during the first postnatal month, during the period of intensive growth of CA3 pyramidal neurons (Gaiarsa et al. 1992; Gomez-Di Cesare et al. 1997).

Similar to the gramicidin perforated patch, depolarized values of the membrane potential have been obtained in neonatal neurons using whole cell recordings. At P2–3, the resting membrane potential was -58 ± 3 mV, input resistance was 1.4 ± 0.1 GΩ, and capacitance was 48 ± 5 pF ($n = 20$). Interestingly, the E_m value strongly depended on seal resistance measured in cell-attached configuration prior to whole cell formation: in cells with seal resistance <10 GΩ (on average, 5.5 ± 0.8 GΩ) the E_m value was -50 ± 3 mV ($n = 10$); in cells with seal resistance >10 GΩ (on average, 13.9 ± 3.1 GΩ), the E_m value was -65 ± 3 mV ($n = 10$).

Cell-attached recordings of NMDA channels

In the next series of experiments, we estimated the value of the membrane potential from cell-attached recordings of NMDA channels. The rationale of this approach is based on the fact that currents through NMDA channels reverse near 0 mV (Nowak et al. 1984), and therefore in cell-attached recordings, NMDA currents should reverse their polarity at a holding potential on the pipette $V_p = E_m$. Figure 3 shows examples of

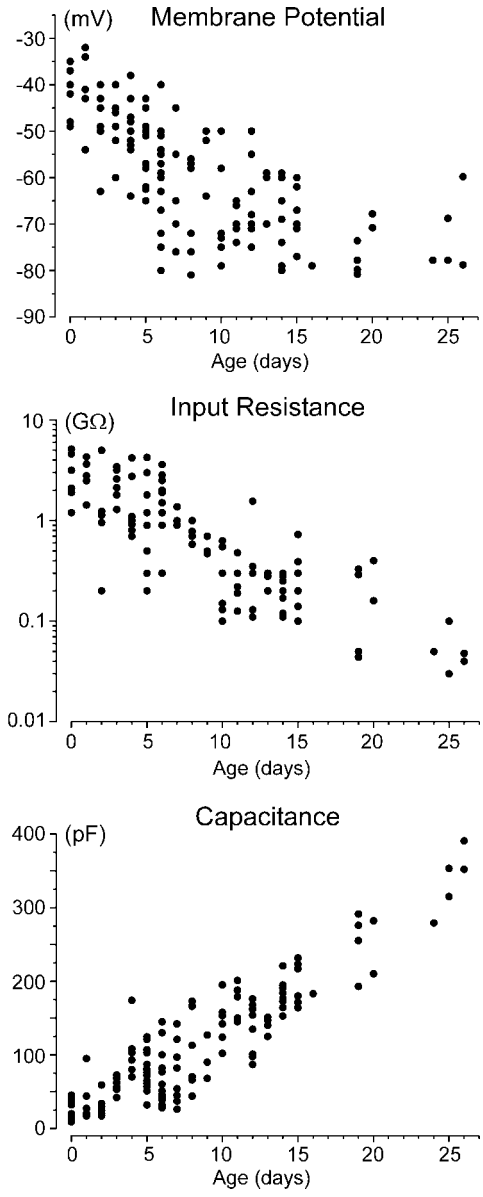

FIG. 2. The membrane potential, input resistance, and capacitance of CA3 pyramidal cells during their postnatal development measured using gramicidin perforated-patch recordings. Each point represents one cell. Pooled data were obtained from 108 neurons. Note that with age, the membrane potentials become more negative, the input resistances decrease, and the capacitances increase.

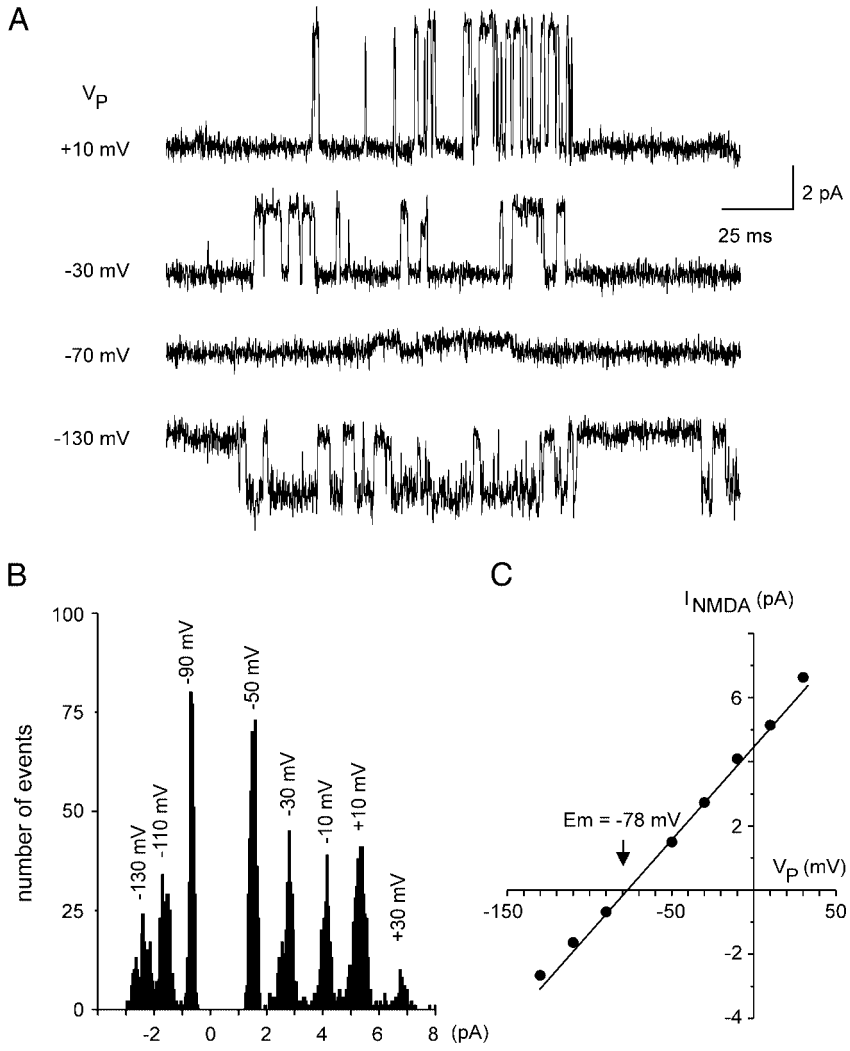

FIG. 3. The membrane potential determined from cell-attached recordings of *N*-methyl-D-aspartate (NMDA) channels. Cell-attached recordings of NMDA channels from a P2 CA3 pyramidal cell at various pipette potentials (V_p); note that upward openings in cell-attached mode correspond to inward currents. Histograms of the amplitudes of currents through single NMDA channels at different pipette potentials. Current-voltage relationship of NMDA channels recorded in cell-attached mode. Note that currents through NMDA channels reverse at $V_p = -78$ mV; assuming that NMDA receptor-mediated currents reverse at a membrane potential of 0 mV, resting membrane potential of this cell should be −78 mV.

currents through NMDA channels recorded in cell-attached configuration from CA3 pyramidal cell at P2 at different values of V_p. Currents through NMDA channels reversed at $V_p = -77 \pm 2$ mV at P2 ($n = 9$), that is, by 29 mV more negative than E_m value obtained at P2 using gramicidin perforated-patch recordings (-48 ± 3 mV; $n = 6$).

Knowing the conductance of NMDA channels from the current-voltage curve, one can further use cell-attached recordings of NMDA channels to monitor the dynamic changes of the membrane potential according to a formula: $E_m = V_p - I_{NMDA}/\gamma$, where γ is a conductance of NMDA channel and I_{NMDA} is an amplitude of current through the NMDA channel at a given V_p. Figure 4 shows simultaneous cell-attached recordings of NMDA channels from CA3 pyramidal cell and field potential recordings from CA3 pyramidal cell layer in a P2 hippocampal slice. In all four pyramidal cells recorded in this series, we observed depolarization sags culminating in bursts of action currents synchronous with giant depolarizing potentials (GDPs) (Ben-Ari et al. 1989) recorded with an extracellular electrode as a spontaneous population burst of multiple-unit activity (MUA; Fig. 4*C*).

Similar recordings performed at P13–14 also revealed spontaneous, often regular, fluctuations of the membrane potential sometimes associated with bursts of action currents (Fig. 5). However, in contrast to the activity in younger hippocampal slices, fluctuations of the membrane potential and action currents were not correlated with MUA (Fig. 5*C*). This result is in agreement with cessation of the immature pattern of GDPs at P10–12 (Ben-Ari et al., 1989). The average membrane potential of P13–14 CA3 pyramidal cells deduced from cell-attached recordings of NMDA channels was −77 ± 2 mV ($n = 6$). This value is not significantly different from E_m estimated using the same approach at P2 but is 10 mV more negative than the E_m value obtained using gramicidin perforated patch recordings from age-matched pyramidal cells (−67 ± 2 mV; $n = 12$).

Dual patch-clamp recordings

In the next series of experiments, we attempted to determine the impact of whole cell recordings on the membrane potential using dual patch-clamp recordings from the soma of the same neuron. In this series, the E_m value measured with a single electrode in whole cell mode was −53 ± 4 mV ($n = 6$; P5). Breaking into whole cell configuration with the second electrode caused neuronal depolarization to −37 ± 4 mV ($n = 6$). These results suggest that whole cell recordings are associated with depolarization of the immature neurons.

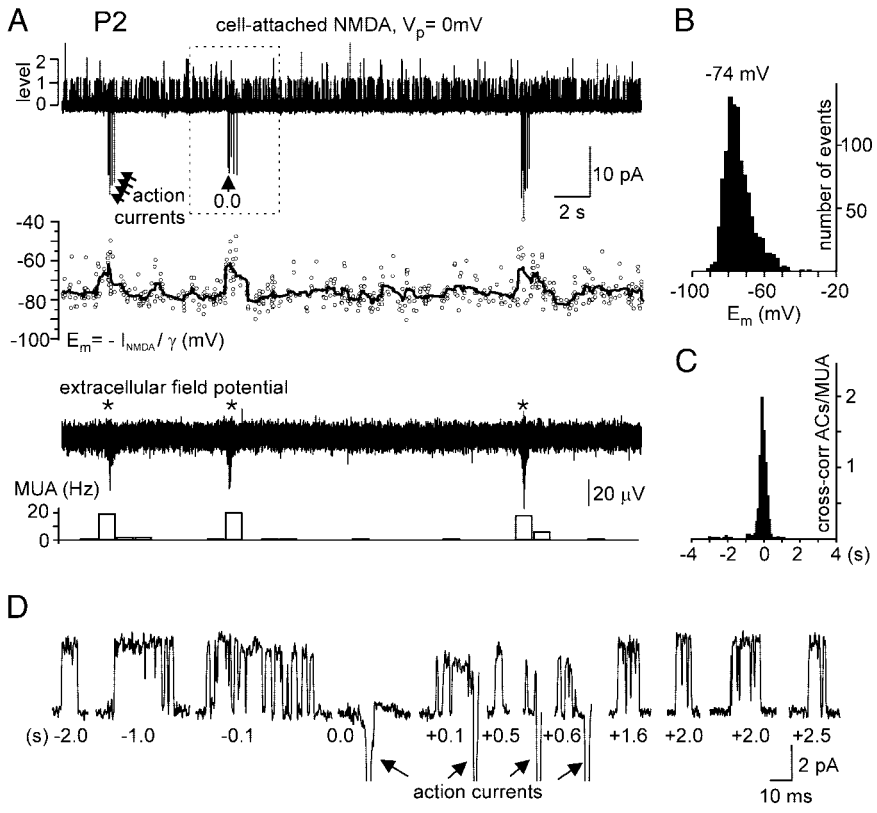

FIG. 4. Monitoring of the membrane potential in P2 CA3 hippocampal neuron using cell-attached recordings of NMDA channels. *A, top*: cell-attached recordings of NMDA channels from a P2 CA3 pyramidal cell at 0 mV pipette potential; note that the patch contains several channels whose superposition gives several levels of current from the baseline (marked as 0). Downward deflections from the baseline are bursts of action currents. Part of the trace outlined with a dashed box is shown on expanded time scale on *D*. *Middle top*: the values of membrane potential (E_m) deduced from the amplitude of currents through NMDA channels (1-level openings) as $E_m = V_p - \gamma/I_{NMDA}$. Solid line represents a fit with a running average of 10 adjacent points. Note membrane depolarizations associated with bursts of action currents. *Bottom*: simultaneous recordings of the extracellular field potential in the pyramidal cell layer of the CA3 subfield. *Middle bottom*: a running average frequency of MUA (bin: 1 s). Note that sags of depolarization and action currents in the pyramidal cell above are synchronized with GDPs in extracellular field recordings (marked by asterisks). *B*: Frequency histogram of E_m values deduced from the amplitudes of currents through single NMDA channels. Mean value of E_m is –74 mV. *C*: cross-correlation of times of action currents in the pyramidal cell versus times of multiple-unit activity (MUA). Note that activity of the pyramidal cell is highly synchronized with population activity in giant depolarizing potentials (GDPs). *D*: examples of NMDA channel openings at various times of the population burst (trace from the *A* outlined with a dashed box). Note reduction of the amplitude of current through the NMDA channel during the population burst that probably reflects membrane depolarization.

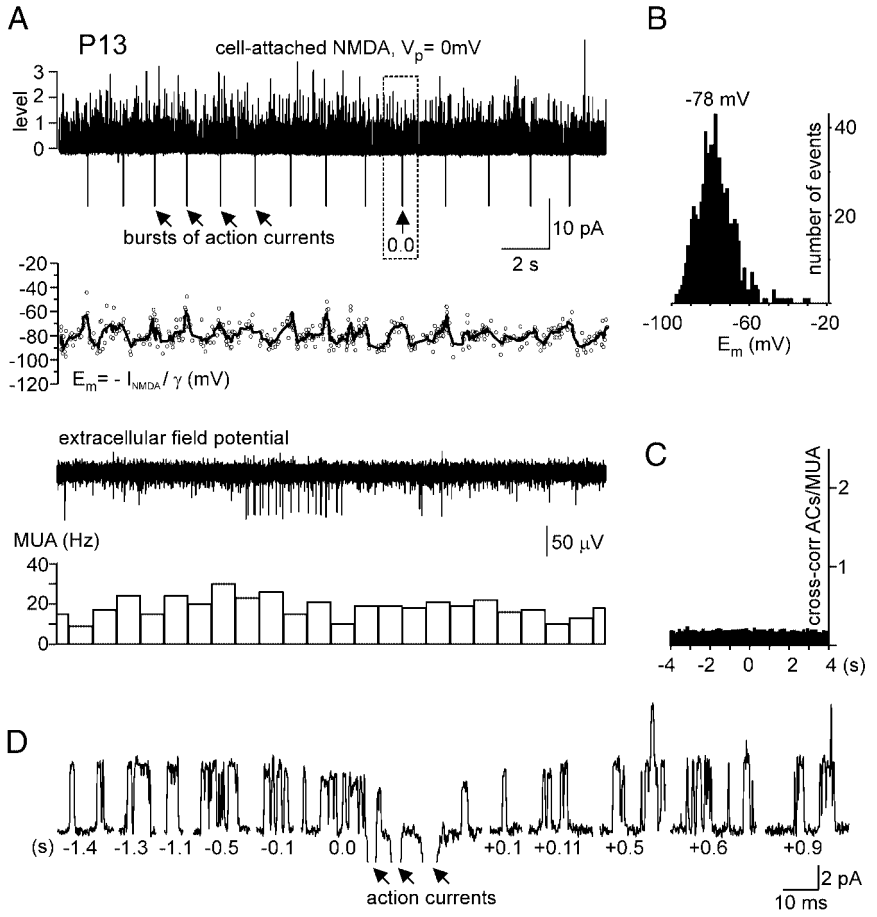

FIG. 5. Monitoring of the membrane potential in a spontaneously bursting CA3 pyramidal cell at P13 using NMDA channels in cell-attached recordings as a voltage sensor. *A, top*: cell-attached recordings of NMDA channels from a P13 CA3 pyramidal cell at 0 mV pipette potential; note that patch contains several channels whose superposition gives several levels of current from the baseline (marked as 0). Downward deflections from the baseline are bursts of 3 action currents. Part of the trace outlined with a dashed box is shown on expanded time scale on *D*. *Middle top*: values of membrane potential (E_m) that were deduced from the amplitude of currents through NMDA channels according to a formula $E_m = V_p - \gamma/I_{NMDA}$. Note the membrane potential oscillations that are phase locked with bursts of action currents. *B*: frequency histogram of E_m values deduced from the amplitudes of currents through single NMDA channels. Mean value of E_m is around –78 mV. *C*: cross-correlation of times of action currents in the pyramidal cell vs. times of MUA. Note that activity of the pyramidal cell is not correlated with a population activity. *D*: 1 cycle of membrane potential oscillations is shown on expanded time scale (trace from the *A* outlined with a dashed box). Examples of NMDA channel openings at various times from the burst of action currents (time of burst is taken as a reference).

Simulations

Thus in gramicidin perforated-patch and whole cell recordings, membrane potentials were significantly more depolarized than in cell-attached recordings of NMDA channels. The difference was most prominent in immature neurons. In keeping with the artifacts of measurements of the membrane potential in small neurons (Barry and Lynch 1991), we attempted to estimate the contribution of short circuit effect of the leak conductance between the cell membrane and patch pipette to membrane potential in whole cell and perforated-patch recordings.

For simulations, we used one-compartment model (Barry and Lynch 1991), the electric scheme of which is shown on Fig. 6. Cell is represented by whole cell membrane resistance (R_m), capacitance (C_m), and battery (E^0_m), which equals the resting potential of the intact cell. The seal contact between the patch-pipette and membrane is considered as a shunt conductance $1/R_{ps}$ with a reversal potential E_{ps} equal to the liquid junction potential between the pipette and bath solutions. The input resistance of the amplifier was considered to be infinitively high. In the stationary state, the sum of all currents is null

$$\frac{E'_m - E^0_m}{R_m} + \frac{E'_m - E_{ps}}{R_{ps}} = 0 \qquad (1)$$

where E'_m is an apparent membrane potential on the input of amplifier and

$$E'_m = \frac{E^0_m \cdot R_{ps} + E_{ps} R_m}{R_{ps} + R_m}$$

Connected in parallel to the cell, seal conductance introduces an error in measurement of the cell input resistance. Although R_m cannot be measured experimentally, it can be estimated from the experimentally measured values of R_{ps} and input resistance R_{in}. R_{in} is a result of a parallel connection of R_{ps} and R_m

$$R_{in} = \frac{R_m \cdot R_{ps}}{R_m + R_{ps}} \quad \text{so} \quad R_m = \frac{R_{in} \cdot R_{ps}}{R_{ps} - R_{in}}$$

Using this expression of R_m, *Eq. 1* is transformed to an equation that couples real and measured values of membrane potential

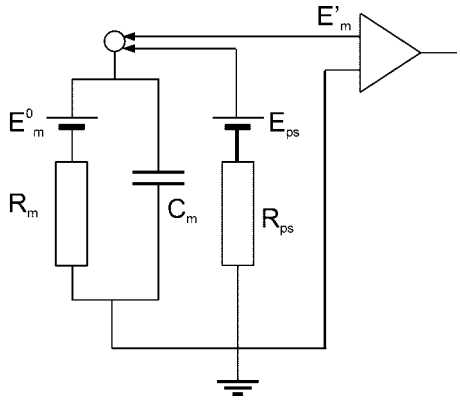

FIG. 6. Circuit diagram of patch-clamp recordings that includes the shunt through the seal between the pipette and membrane. Cell is presented by the whole cell resistance (R_m), capacitance (C_m), and the cell equilibrium potential (E^0_m) that corresponds to the membrane potential of the intact cell. The seal contact is presented by shunt resistance (R_{ps}) and the liquid junction potential between the pipette and extracellular solutions (E_{ps}).

$$E'_m = E^0_m \frac{R_{ps} - R_{in}}{R_{ps}} + E_{ps} \frac{R_{in}}{R_{ps}} \qquad (2)$$

In our simulations, E^0_m was deduced from cell-attached recordings of NMDA channels, and R_{ps} and R_{in} were measured in cell-attached and whole cell/perforated-patch recordings, respectively.

According to *Eq. 2*, the closer the seal resistance R_{ps} is to R_{in}, the more depolarized should be the apparent membrane potential (E'_m). We therefore compared the dependence of E'_m on the ratio R_{in}/R_{ps}. We assumed that the real membrane potential E^0_m equals −77 mV—the value deduced from cell-attached recordings. The reversal potential of the current through the seal, E_{ps}, was considered as the liquid junction potential between the pipette and bath solutions, −7 mV in whole cell recordings and −1 mV in gramicidin perforated-patch recording.

The experimentally measured membrane potentials in perforated-patch (*A*) and whole cell recordings (*B*) are plotted as a function of R_{in}/R_{ps} in Fig. 7, together with theoretical prediction for the corrupted membrane potential derived from the *Eq. 2*. When $R_{in} \ll R_{ps}$ and ratio R_{in}/R_{ps} approximates zero, the simulated membrane potential approximates the value of E^0_m, −77mV. When R_{in} approaches R_{ps} and ratio R_{in}/R_{ps} approximates 1, the simulated membrane potential approximates the reversal potential of the seal shunting conductance. There is a trend of the experimentally measured membrane potentials to depolarize with an increase of R_{in}/R_{ps} ratio. The coefficient of correlation between the experimental data and the results of simulation was 0.55 and 0.59 for perforated-patch and whole cell recordings, respectively.

DISCUSSION

The principal findings of the present study are as follows: *1*) when measured using gramicidin perforated-patch and whole cell recordings, the membrane potential of neonatal CA3 pyramidal cells is strongly depolarized to −44 mV; during the two first postnatal weeks, the membrane potential progressively shifts to −67 mV; *2*) when measured using cell-attached recordings of NMDA channels, the membrane potential of neonatal and 2-wk-old CA3 pyramidal cells does not significantly differ (about −77 mV); and *3*) results of simulation studies reveal that the apparent depolarized values of the membrane potential with perforated-patch and whole cell recordings are due to the short-circuit effect of the shunt through the seal contact between the patch pipette and the membrane. This error is most important in small neurons with high resistances.

Our finding of depolarized values of the membrane potential in neonatal CA3 pyramidal cells obtained using perforated-patch and whole cell recordings is in agreement with previous developmental studies that employed perforated-patch, whole cell and intracellular recordings in the hippocampus and other brain regions (see INTRODUCTION). Strongly depolarized values of the membrane potential should have a major impact on neuronal excitability. In particular, depolarized membrane potentials in the immature neurons could contribute to increased neuronal excitability to provide activation of voltage-gated calcium channels and influx of calcium necessary for neuronal growth at early developmental stages when the number of excitatory synapses is low; increased contribution of NMDA

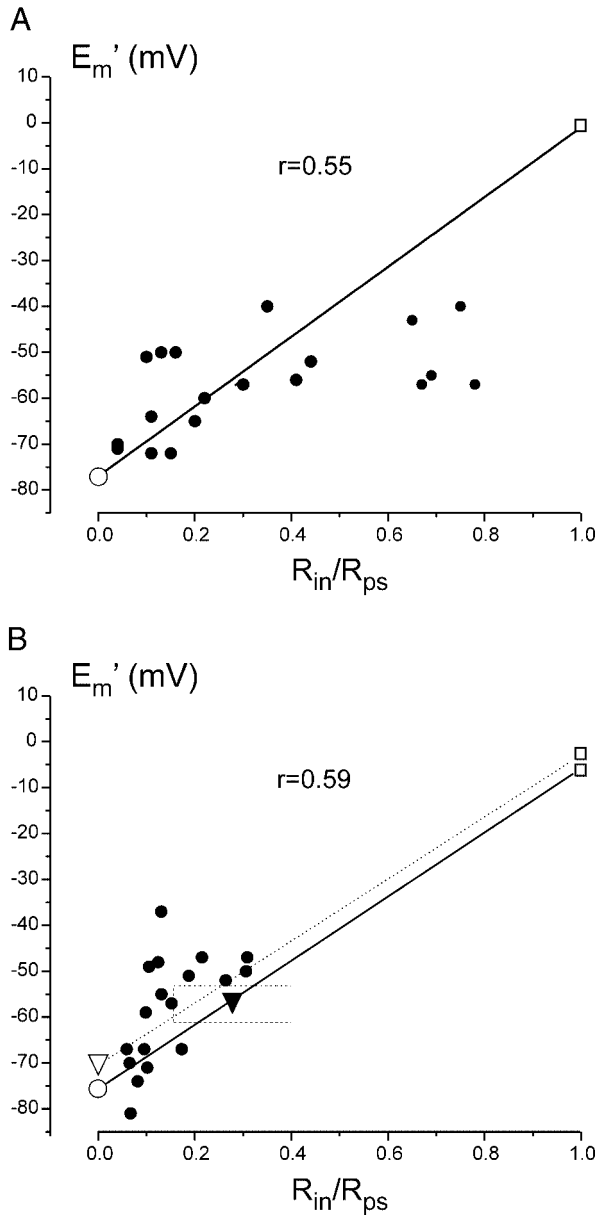

FIG. 7. Dependence of the average membrane potential on the ratio between the input and seal resistances. The average membrane potentials measured using perforated-patch (*A*) and whole cell (*B*) recordings as a function of the ratio R_{in}/R_{ps}. —, the theoretical predictions for the membrane potentials according to equation $E'_m = E^0_m(R_{ps} - R_{in})/R_{ps} + E_{ps}R_{in}/R_{ps}$ that is based on the model of seal resistance operating as a shunt (see also Fig. 6 and RESULTS for details). ○, the membrane potential of –77 mV obtained from cell-attached recordings of NMDA channels; it was also taken as E^0_m. □, the liquid junction potentials. *B*: ▽ and ▼, the average membrane potentials measured in cell-attached and whole cell configurations, respectively; - - -, the range of the measured in whole cell membrane potentials and corresponding values of R_{in}/R_{ps}; · · ·, a theoretical prediction for the dependence of the apparent membrane potential on R_{in}/R_{ps} derived from the data was presented in the article by Fricker et al. (1999).

receptors to synaptic responses in the immature neurons; increased excitability of the immature networks manifested by spontaneous synchronized neuronal discharges (GDPs in the hippocampus) as well as a higher propensity of the immature brain to seizures. It has also been speculated that depolarized potential of the immature neurons could contribute to programmed neuronal death (Luhmann et al. 2000). However, there are several lines of evidence that argue that the depolarized values of the membrane potential in immature neurons are due to a technical error associated with whole cell and perforated-patch recordings: cell-attached recordings of NMDA channels failed to reveal any developmental change in the membrane potential of CA3 pyramidal cells; in perforated-patch and whole cell recordings, neonatal CA3 pyramidal neurons were in a state of depolarization block, whereas in cell-attached recordings, neonatal neurons reliably fired action potentials; dual whole cell recordings from the immature neurons revealed a significant neuronal depolarization after addition of the second whole cell electrode; while most of neuronal firing is synchronized in GDPs and neurons fire action potentials with a high probability during GDPs in cell-attached or extracellular recordings during the first postnatal week (Fig. 4) (see also (Ben-Ari et al. 1989; Leinekugel et al. 1997), firing of pyramidal cells during GDPs in whole cell and perforated-patch recordings during the first postnatal week was clearly abnormal. Taken together, these observations support the hypothesis that the depolarized membrane potential of neonatal neurons is not a physiological phenomenon but rather an artifact of invasive measurements.

Using noninvasive cell-attached recordings of NMDA channels, we found that the membrane potential of CA3 pyramidal cells does not change during development and is more polarized than that obtained using whole cell or perforated-patch recordings. Estimation of membrane potential from cell-attached recordings of NMDA channels has a number of advantages over conventional invasive techniques including perforated-patch, whole cell, and intracellular sharp electrode recordings: the neuronal membrane remains intact and therefore no leak conductance is introduced; the composition of cytoplasm and the activity of ionic channels are unaltered; and a liquid junction potential does not develop between the pipette solution and cytoplasm. Noninvasive cell-attached measurements of membrane potential may employ not only NMDA channels but also any other type of channels with known reversal potential. Thus membrane potential has been estimated recently using cell-attached recordings of potassium channels in CA1 pyramidal cells and interneurons (Fricker et al. 1999; Verheugen et al. 1999) and interestingly, the authors also found 13 mV more hyperpolarized value of the membrane potential in cell-attached recordings comparing to whole cell recordings.

The key issue in the cell-attached approach for the measurements of membrane potential is the reversal potential of the conductance that is used as a voltage sensor. We assumed that the reversal potential of NMDA currents is 0 mV. However, this value has been obtained using invasive recordings (Nowak et al. 1984), whereas E_{NMDA} in the intact cell is unknown. NMDA currents are equally permeable to K^+ and Na^+, and therefore E_{NMDA} is determined by their total extra- and intracellular activities. In the external solution, total concentration of K^+ and Na^+ is 155 mM; with the activity coefficient of 0.85, it gives 131 mM of free K^+ and Na^+. In the intracellular solution, the activity of K^+ in the hypoglossal neurons was estimated using ion-selective electrodes as 96 mM (Jiang and Haddad 1991) and free Na^+ concentration in hippocampal neurons was estimated using fluorescent sodium indicator SFBI as 10 mM (Diarra et al. 2001), giving 106 mM of total free K^+ and Na^+. Relatively low activity of the intracellular

cations comparing to that of the extracellular cations is probably due to lower activity coefficients of the salts made with relatively weak intracellular organic acids. According to Nernst equation, the reversal potential of currents through NMDA channels in the intact cell should be around +5 mV. Corrected for this error, E_m should equal −82 mV.

Currents through NMDA channels may alter membrane potential and introduce a potential error in the estimation of the membrane potential. It has been demonstrated that in small neurons, openings of single channels produce significant changes in neuronal potential and can even trigger action potentials (Barry and Lynch 1991). The effect of the current through the channel on membrane potential depends on cell capacitance and resistance. In our recording conditions, the membrane potential is estimated from the current-voltage relationship as a voltage on the pipette at which the current through NMDA channel is null; therefore the activity of channels should not affect the estimate of the membrane potential. The error may occur when current flows through NMDA channel. Thus in the case of monitoring of the dynamic changes of the membrane potential using NMDA channels as a voltage sensor at $V_p = 0$ mV (Fig. 4 and 5), inward current through NMDA channels should induce neuronal depolarization. In immature neurons with low capacitance and high membrane resistance, this depolarization should be the most prominent; however, we calculated that even at P2, with $C_m =$ 35 pF and $R_m = 2.5$ GΩ, 5-ms openings of NMDA channel should produce depolarization of ~1 mV. Similar calculations for P13–14 neurons indicate that depolarization produced by opening of single NMDA channel in cell-attached patch at $V_p = 0$ mV is ~0.2 mV. Thus currents through single NMDA channel in cell-attached recordings induce little change of the membrane potential of postnatal CA3 pyramidal cells.

The results of the present study are in agreement with the work of Barker and colleagues (Maric et al. 1998) in which noninvasive potentiometric techniques have been employed to determine the resting membrane potential of the acutely dissociated cortical neurons at E11–22. In their study, the value of resting membrane potential of postmitotic cortical neurons at E18 was estimated at −86 ± 4 mV using oxonol measurements and at −80 ± 7 mV using videoimaging technique, while with perforated patch recordings the membrane potential was −60.8 ± 6.5 mV, that is, 20–25 mV more depolarized. As with the present study, the authors suggested that the depolarized value of the membrane potential in perforated-patch recordings is due to the error associated with recordings from small cells.

Comparing the experimental results with theoretical calculations indicates that leakage introduced in whole cell and perforated-patch recordings can be the principal factor determining the depolarized value of the membrane potential in the immature CA3 pyramidal neurons. At the same time, we observed large deviations in the experimental data from the theoretical curve, which considers leak resistance parallel to membrane resistance (Fig. 7). These deviations can be due to several factors. *1*) Our simple model does not include active membrane properties. For example, it is conceivable that negative deflection from prediction in several cells with high R_{in}/R_{ps} (Fig. 7*A*) is due to activation of voltage-gated potassium conductance. *2*) The value of R_{ps} is estimated in cell-attached mode whereas this parameter might undergo undefined change after transition to whole cell mode. *3*) R_{ps} may be actually underestimated in the perforated-patch recordings because of traces of gramicidin in the tip solution during cell-attach formation.

The present results have been obtained in the absence of any pharmacological blocker; therefore synaptic activity and interplay of the voltage-gated channels both contributed to the average membrane potential. In our previous study (Leinekugel et al. 1997), a similar technique of cell-attached recordings of NMDA channels was employed to determine the effects of GABA on the activity of NMDA channels in P2–5 CA3 pyramidal cells. In that study, recordings were performed in the presence of tetrodotoxin to suppress ongoing activity and GDPs. Estimated from the reversal potential of currents through NMDA channels in cell-attached mode, the resting membrane potential of CA3 pyramidal cells was −84 ± 3 mV, 7 mV more hyperpolarized compared with the value obtained in the present study. It is likely that ongoing synaptic activity and GDPs (Fig. 4), as well as intrinsic membrane potential oscillations (Fig. 5), contribute to depolarized value of the average membrane potential in control conditions. Interestingly, the value of −84 mV matches the estimate of the membrane potential in "silent" CA1 pyramidal cells of P11–26 rats (also −84 mV) from the reversal of currents through potassium channels in cell-attached configuration in the presence of antagonists of ionotropic GABA and glutamate receptors (Fricker et al. 1999). Corrected for hypothetical $E_{NMDA} = +5$ mV in the intact cell (see preceding text), the membrane potential of CA3 pyramidal cell in the presence of tetrodotoxin equals −89 mV, which matches the reversal potential of potassium conductance of −88 mV estimated from the free concentrations of potassium inside (96 mM (Jiang and Haddad 1991) and outside the cell (0.85 · 3.5 mM = 2.9 mM).

Results of theoretical simulations indicate that the error associated with leak conductance is most apparent in neonatal CA3 pyramidal neurons. However, a significant error was also predicted for measurements of the membrane potential in more mature neurons. Thus we found 10-mV difference between the membrane potential of CA3 pyramidal cells at P13–14 when measured using perforated-patch recordings (−67 mV) and the membrane potential deduced from the reversal potential of currents through NMDA channels (−77 mV). Miles and colleagues also found ~13 mV difference in the membrane potential estimated from the reversal potential of the currents through potassium channels in cell-attached configuration and whole cell recordings from P11–26 CA1 pyramidal cells (Fricker et al. 1999). We attempted to calculate the leak error that could have affected the values of the membrane potential in whole cell recordings in the latter study by using the following values: $R_{ps} = 1$ GΩ; $R_{in} = 150–400$ MΩ; $E_m^0 = -70$ mV. Under these conditions, 10–27 mV of the depolarization are secondary to a leak error (see also Fig. 7). The range of the expected membrane potentials at given values of R_{in}/R_{ps} is outlined by the dashed box on Fig. 7.

In the present study, we compared the membrane potentials deduced from cell-attached recordings of NMDA channels and directly measured using whole cell or gramicidin perforated-patch recordings in different sets of cells. Further experiments with dual cell-attached and whole cell recordings from the same neuron can provide more precise estimation of the impact of short-circuit effect of the whole cell approach.

Taken together, the results of the present study suggest that developmental changes in the resting membrane potential of CA3 pyramidal cells are primarily due to the leak that is introduced in intracellular, whole cell, and perforated-patch recordings; leak error may alter measurements of the membrane potential in both mature and immature neurons; obtaining seal resistances much higher than cell resistance will diminish this artifact; and the membrane potential of CA3 pyramidal cells appears to be strongly negative at birth and does not change during postnatal development. Despite a tremendous change in resting conductance, and the widely documented changes in ion channel expression, the absolute level of resting membrane potential is almost constant during postnatal development.

We thank Dr. R. Miles for the useful suggestions at the beginning of this study and Drs. K. Kaila, I. Medina, T. Launey, A. Savchenko, D. Debanne, and D. Rusakov for the critical reading of the manuscript.

DISCLOSURES

Financial support for this study from Institut de la Santé et de la Recherche Médicale, Fondation pour La Recherche Médicale, National Institute of Neurological Disorders and Stroke Grant NS-27984, International Brain Research Organization, and Ligue Francaise Contre e'Epilepsie is acknowledged.

REFERENCES

Anderson RL, Jobling P, and Gibbins IL. Development of electrophysiological and morphological diversity in autonomic neurons. *J Neurophysiol* 86: 1237–1251, 2001.

Barry PH and Lynch JW. Liquid junction potentials and small cell effects in patch-clamp analysis. *J Membr Biol* 121: 101–117, 1991.

Belleau ML and Warren RA. Postnatal development of electrophysiological properties of nucleus accumbens neurons. *J Neurophysiol* 84: 2204–2216, 2000.

Ben-Ari Y, Cherubini E, Corradetti R, and Gaiarsa JL. Giant synaptic potentials in immature rat CA3 hippocampal neurons. *J Physiol* 416: 303–325, 1989.

Ben-Ari Y, Khazipov R, Leinekugel X, Caillard O, and Gaiarsa JL. GABA-A, NMDA, and AMPA receptors: a developmentally regulated "menage a trois." *Trends Neurosci* 20: 523–529, 1997.

Burgard EC and Hablitz JJ. Developmental changes in NMDA and non-NMDA receptor-mediated synaptic potentials in rat neocortex. *J Neurophysiol* 69: 230–240, 1993.

Diarra A, Sheldon C, and Church J. In situ calibration and [H+] sensitivity of the fluorescent Na^+ indicator SBFI. *Am J Physiol Cell Physiol* 280: C1623–C1633, 2001.

Ebihara S, Shirato K, Harata N, and Akaike N. Gramicidin-perforated patch recording: GABA response in mammalian neurones with intact intracellular chloride. *J Physiol* 484: 77–86, 1995.

Fricker D, Verheugen JA, and Miles R. Cell-attached measurements of the firing threshold of rat hippocampal neurones. *J Physiol* 517: 791–804, 1999.

Gaiarsa JL, Beaudoin M, and Ben-Ari Y. Effect of neonatal degranulation on the morphological development of rat CA3 pyramidal neurons: inductive role of mossy fibers on the formation of thorny excrescences. *J Comp Neurol* 321: 612–625, 1992.

Gomez-Di Cesare CM, Smith KL, Rice FL, and Swann JW. Axonal remodeling during postnatal maturation of CA3 hippocampal pyramidal neurons. *J Comp Neurol* 384: 165–180, 1997.

Horn R and Marty A. Muscarinic activation of ionic currents measured by a new whole-cell recording method. *J Gen Physiol* 92: 145–159, 1988.

Jiang C and Haddad GG. Effect of anoxia on intracellular and extracellular potassium activity in hypoglossal neurons in vitro. *J Neurophysiol* 66: 103–111, 1991.

Khazipov R, Ragozzino D, and Bregestovski P. Kinetics and Mg2+ block of *N*-methyl-D-aspartate receptor channels during postnatal development of hippocampal CA3 pyramidal neurons. *Neuroscience* 69: 1057–1065, 1995.

Lamsa K, Palva JM, Ruusuvuori E, Kaila K, and Taira T. Synaptic GABA(A) activation inhibits AMPA-kainate receptor-mediated bursting in the newborn (P0–P2) rat hippocampus. *J Neurophysiol* 83: 359–366, 2000.

Leinekugel X, Medina I, Khalilov I, Ben-Ari Y, and Khazipov R. Ca^{2+} oscillations mediated by the synergistic excitatory actions of GABA(A) and NMDA receptors in the neonatal hippocampus. *Neuron* 18: 243–255, 1997.

LoTurco JJ, Blanton MG, and Kriegstein AR. Initial expression and endogenous activation of NMDA channels in early neocortical development. *J Neurosci* 11: 792–799, 1991.

Luhmann HJ, Reiprich RA, Hanganu I, and Kilb W. Cellular physiology of the neonatal rat cerebral cortex: intrinsic membrane properties, sodium and calcium currents. *J Neurosci Res* 62: 574–584, 2000.

Maric D, Maric I, Smith SV, Serafini R, Hu Q, and Barker JL. Potentiometric study of resting potential, contributing K^+ channels and the onset of Na^+ channel excitability in embryonic rat cortical cells. *Eur J Neurosci* 10: 2532–2546, 1998.

Martin-Caraballo M and Greer JJ. Electrophysiological properties of rat phrenic motoneurons during perinatal development. *J Neurophysiol* 81: 1365–1378, 1999.

Marty A and Neher E. Tight-seal whole-cell recording. In: *Single Channel Recording*, edited by Sakmann B and Neher E. New York: Plenum, p. 31–52.

Masetto S, Perin P, Malusa A, Zucca G, and Valli P. Membrane properties of chick semicircular canal hair cells in situ during embryonic development. *J Neurophysiol* 83: 2740–2756, 2000.

Mienville JM and Pesold C. Low resting potential and postnatal upregulation of NMDA receptors may cause Cajal-Retzius cell death. *J Neurosci* 19: 1636–1646, 1999.

Nowak L, Bregestovski P, Ascher P, Herbert A, and Prachiantz A. Magnesium gates glutamate-activated channels in mouse central neurones. *Nature* 307: 462–465, 1984.

Psarropoulou C and Descombes S. Differential bicuculline-induced epileptogenesis in rat neonatal, juvenile, and adult CA3 pyramidal neurons in vitro. *Brain Res Dev Brain Res* 117: 117–120, 1999.

Spiegelman I, Zhang L, and Carlen PL. Patch-clamp study of postnatal development of CA1 neurons in rat hippocampaal slices: membrane excitability and K^+ currents. *J Neurophysiol* 68: 55–69, 1992.

Spitzer NC. Ion channels in development. *Annu Rev Neurosci* 2: 363–397, 1979.

Spruston N and Johnston D. Perforated patch-clamp analysis of the passive membrane properties of three classes of hippocampal neurons. *J Neurophysiol* 67: 508–529, 1992.

Staley KJ, Otis TS, and Mody I. Membrane properties of dentate gyrus granule cells: comparison of sharp microelectrode and whole-cell recordings. *J Neurophysiol* 67: 1346–1358, 1992.

Velumian AA, Zhang L, Pennefather P, and Carlen PL. Reversible inhibition of IK, IAHP, Ih and ICa currents by internally applied gluconate in rat hippocampal pyramidal neurones. *Pfluegers* 433: 343–350, 1997.

Verheugen JA, Fricker D, and Miles R. Noninvasive measurements of the membrane potential and GABAergic action in hippocampal interneurons. *J Neurosci* 19: 2546–2555, 1999.

Wang YF, Gao XB, and van den Pol AN. Membrane properties underlying patterns of GABA-dependent action potentials in developing mouse hypothalamic neurons. *J Neurophysiol* 86: 1252–1265, 2001.

Zhang L, Spigelman I, and Carlen PL. Development of GABA-mediated, chloride-dependent inhibition in CA1 pyramidal neurones of immature rat hippocampal slices. *J Physiol* 444: 25–49, 1991.

Zhou FM and Hablitz JJ. Postnatal development of membrane properties of layer I neurons in rat neocortex. *J Neurosci* 16: 1131–1139, 1996.